Progress In Electromagnetics Research, PIER 85, 261–288, 2008

EM FULL-WAVE ANALYSIS AND TESTING OF NOVEL QUASI-ELLIPTIC MICROSTRIP FILTERS FOR ULTRA NARROWBAND FILTER DESIGN

Z. M. Hejazi †

Department of Communication Engineering
Hijjawi Faculty of Engineering Technology
Yarmouk University
Irbid, Jordan

M. C. Scardelletti

NASA Glenn Research Center
USA

F. W. Van Keuls

Ohio Aerospace Institute
NASA Glenn Research Center
USA

A. A. Omar

Department of Communication Engineering
Hijjawi Faculty of Engineering Technology
Yarmouk University
Irbid, Jordan

A. Al-Zayed

Electrical Engineering Department
Kuwait University
Kuwait

† On leave with the Department of Electronics and Communication, Middle East College of Information Technology (MECIT), Muscat, Oman

Abstract—A new class of microstrip filter structures are designed, optimized, simulated and measured for ultra-narrowband performance essential to the wireless industry applications. More accurate model of the coupling coefficient is outlined and tested for narrowband filter design. Two sample filters are fabricated and measured to verify the simulations and prove the concept. The idea behind the new designs is based on minimizing the parasitic couplings within the resonators and the inter-resonator coupling of adjacent resonators. A reduction of the overall coupling coefficient is achieved even with less resonator separation which is a major issue for compactness of such filters. The best new designs showed a simulated fractional bandwidth (FBW) of 0.05% and 0.02% with separations of $S = 0.63\,\text{mm}$ and $S = 0.45\,\text{mm}$, respectively. The measured filters tend to have even narrower FBW than the simulated, though its insertion loss deteriorates, possibly due to mismatch at the interface with external circuitry and poor shielding effect of the test platform. The investigated 2-pole filters are accommodated on a compact area of a nearly $0.6\,\text{cm}^2$. An improvement of tens of times of order in narrowband performance is achieved compared to reported similar configuration filters and materials. A sharp selectivity and quasi-elliptic response are also demonstrated with good agreement in both simulations and measurements. In all filters, however, the study shows that the narrower the FBW, the larger the insertion loss (IL) and the worse the return loss (RL). This is confirmed by measurements.

1. INTRODUCTION

Wireless personal communication services (PCS), global system for mobile communications (GSM) and satellite receiver links are some of the important applications which increasingly demand ultra narrowband (NB) filters with a FBW of less than 0.5% and even 0.05%. Such filters should have high selectivity, compact size and smaller weight.

Intensive research efforts have focused on achieving compact low loss NB filters for mobile, wireless and satellites applications with center frequencies (f_o) varying from 965 MHz to 14.25 GHz. A 2-pole hairpin-comp NB microstrip filter for high temperature superconductor (HTS) has been reported by [1] to achieve a FBW of 0.73% at 1 dB points below the minimum attenuation at $f_o = 1.955\,\text{GHz}$, while a similar but a 4-pole filter showed a FBW of 0.94% (1 dB points) at 1.836 GHz. A class of 4-pole cross-coupled microstrip hairpin NB filter have been demonstrated with a FBW of 2.07% at $f_o = 965\,\text{MHz}$ [2]. A NB filter using open-loop resonators with coupled and crossing

lines has also shown about 2% FBW at $f_o = 2.039\,\text{GHz}$ [3]. Several multilayer filter configurations with aperture-coupled microstrip using open-loop resonators have shown a FBW of 4.14% at $f_o = 965\,\text{MHz}$ [4]. A HTS 8-pole microstrip meandered open-loop resonator filter at $f_o = 1738.5\,\text{MHz}$ [5] has shown a much narrower FBW, about 1%, with a quasi-elliptic function response. Another HTS 11-pole hairpin-comp NB microstrip filter has been reported to have a FBW of 0.6% at $f_o = 1.778\,\text{GHz}$ [6]. A 2-pole and 4-pole dual-mode microstrip filters have been demonstrated at a $f_o = 1.39\,\text{GHz}$ with a FBW of 1.36% [7]. A model of a 2-pole tunable microwave NB lumped-element microstrip filter has been developed, using varactor-loaded inductors and showed a possible FBW of 0.5% at $f_o = 980\,\text{MHz}$ [8].

In some recent papers, a FBW of 0.45% at $f_o = 1.774\,\text{GHz}$ is achieved by using a HTS microstrip pseudo-lumped element resonators [9]. A quasi-elliptic 4-pole microstrip filter design at $\approx 2\,\text{GHz}$ has shown a FBW of 0.25%, while a 9-pole filter at 1775 MHz has demonstrated a FBW of 0.84% [10]. Meander-line microstrip resonators [11] also at $f_o = 1775$ have shown a FBW of 0.5%. In the work [12], a filter based on zig-zag hairpin-comp resonators has reported a simulated FBW of 1.46% and a measured FBW of 1.37% at $f_o = 1985\,\text{MHz}$.

Further recent works show the importance of achieving ever narrower bandwidths and higher out-of-band rejection required in the wireless communications industry [13–15], and even in radio astronomy [16]. In one work [15], a HTS microstrip filter, but with lumped-element realization, has shown a possible FBW of 0.014% at a midband frequency of 700 MHz. Microstrip hairpinline narrowband bandpass filter using via ground holes has been presented in [17], where a weak coupling between resonators, while maintaining relatively small spacing between resonators and a FBW of 0.5% to 2.7% is achieved at 1 GHz.

Some most recent paper emphasize on medium FBW with stronger coupling, such as [18], where planar bandpass filters using single patch resonators with corner perturbation cuts are used and a FBW of 13.04% is achieved. Bandpass filters with transmission zeros achieve FBW of 2% at 1 GHz [19]. Microstrip square ring bandpass filters have achieved smaller size but a FBW of 10% at 2 GHz [20]. Bandpass filters with triangular resonators have RL of about 20 dB [21]. FBW of 4% is achieved at 2.4 GHz with compact split ring stepped impedance resonators, while they have RL less than 20 dB and out of band rejection of around 25 dB [22]. Square loop bandpass filters with a FBW of 1.5% but a RL of 10 dB has been reported in [23]. Bandpass filters with isosceles triangular patch resonator have FBW of 9.4% with

RL less than 13 dB [24].

Recent progress in Wideband filters with a FBW beyond 20% and 30% can be found in [25, 26], while ultrawideband filters in [27].

Microstrip configurations for medium and NB microstrip filters, frequently used as basic geometries, are shown in Fig. 1. However, planar ultra NB filters with a FBW of less than 0.1% or 0.05% are still a challenge. This is due to the fact that such filters require a very weak coupling, i.e., a very far apart separation between resonators which on the other hand require a large circuit size. Other challenge is to identify and control the required electric and magnetic nonadjacent cross-couplings to achieve elliptic function response, preferred for its high selectivity due to the transmission zeros near the passband.

In previous works [28, 29], filters with FBWs of 0.08%, 0.05% and 0.02% at wireless frequency, have been initially reported using a new approach in microstrip geometries. Detailed investigation of such type of filters with experimental verification was still needed. This is carried out in this paper with full explanations of the idea behind the new designs. Simulations and measurements are presented at wireless frequency. A model of the coupling coefficient valid for weak coupling cases such as NB filters is outlined. A full-wave EM simulation tool [30] is used to characterize the filters with lossless conductors to simulate the real HTS YBCO conductors on Lanthanum Aluminate ($LaAlO_3$) substrates used in the measurements.

2. MODELING AND SYNTHESIS OF THE FILTER CIRCUITS

A theoretical 2-pole Chebyshev filter is to be synthesized according to given specifications for ultra NB response, i.e., $FBW = 0.05\%$, a passband ripple $r_{pp} = 0.1$ dB and $f_o = 1764$ MHz. The input/output impedances are set to be 50 Ω. A simplified equivalent lumped-element circuit of a bandpass prototype 2-pole filter is shown in Fig. 2.

Using the low-pass to band-pass transformation theory [36], the response of the low pass prototype filter can be related to the response of the bandpass filter as

$$\frac{\omega'}{\omega'_1} = \frac{2}{BW}\left(\frac{\omega - \omega_o}{\omega_o}\right) \tag{1}$$

where ω' and ω'_1 refer to the lowpass response while BW, ω_o, ω_1 and ω_2 refer to the corresponding bandpass filter response related as

$$BW = \left(\frac{\omega_2 - \omega_1}{\omega_o}\right)$$

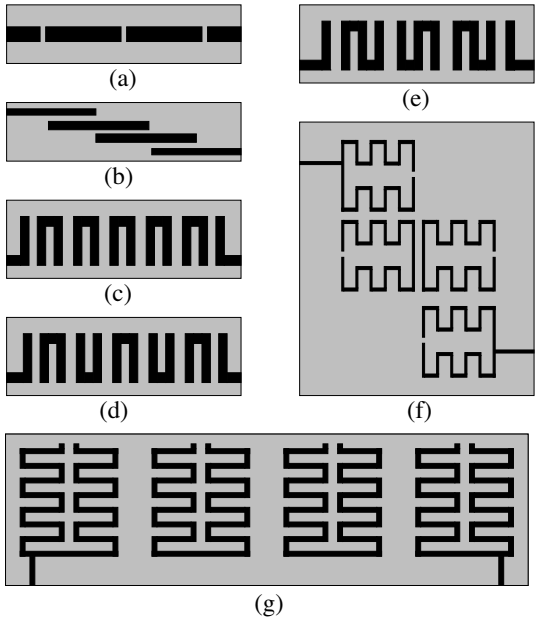

Figure 1. Classical basic geometrical configurations used for medium and NB microstrip filters. (a) Edge-coupled. (b) $\lambda/4$ parallel-coupled. (c) Hairpin-comp. (d) Hairpin. (e) 3-section meander line. (f) Meander open-loop. (g) Zig-zag hairpin-comp resonator filter.

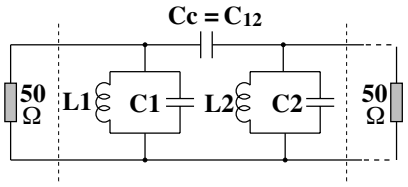

Figure 2. Equivalent lumped-element circuit of the prototype filter.

which represents the bandwidth, and

$$\omega_o = \sqrt{\omega_1 \omega_2}$$

is the midband frequency. ω_1 and ω_2 are the band edge frequencies. For any number of shunt resonators n, the parallel lumped-element values are calculated by

$$C_j = \frac{\omega_1' g_j}{\omega_o BW},\ j = 1, 2, \ldots, n \tag{2}$$

$$L_j = \frac{BW}{\omega_1' \omega_o g_j},\ j = 1, 2, \ldots, n \tag{3}$$

The prototype elements $g_o = 1$, $g_{n+1} = 1$ for odd n and

$$g_{n+1} = \coth^2\left(\frac{\psi}{4}\right)$$

for even n where

$$\psi = \ln\left(\coth\frac{r_{pp}}{17.37}\right)$$

The other elements g_k are computed by

$$g_k = \frac{4a_{k-1}a_k}{b_{k-1}g_{k-1}},\ k = 2, 3, \ldots, n \tag{4}$$

where

$$\begin{aligned} a_k &= \sin\left[\frac{(2k-1)\pi}{2n}\right],\ k = 1, 2, \ldots, n \\ b_k &= \xi^2 + \sin^2\left(\frac{k\pi}{n}\right),\ k = 1, 2, \ldots, n \\ g_1 &= \frac{2a_1}{\xi} \\ \xi &= \sinh\left(\frac{\psi}{2n}\right) \end{aligned}$$

The coupling capacitances $C_{j,\,j+1}$ (in our case only $C_{12} = C_c$) between the resonators can be calculated from the J-inverters as

$$C_{j,\,j+1}\,|_{j=1\ldots n-1} = \frac{J_{j,j+1}}{\omega_o} \tag{5}$$

However, in NB filters, it is difficult to assume only a pure capacitive coupling but also there is an inductive coupling in series with it forming a series resonator. This capacitance alone can be easily adjusted or optimized by the network (circuit model) simulation tool until the split resonances form a flat passband with the specified ripple. If the losses are to be taken into account, which is the case in critical applications [28, 29], the coupling coefficient model was modified for better accuracy as outlined in the next section.

3. A COUPLING COEFFICIENT MODEL FOR NARROWBAND FILTER DESIGN

The coupling coefficient is a crucial parameter in filter design. For the fundamental mode near resonance, an equivalent lumped-element circuit of a 2-pole filter, can be represented by two resonant circuits with identical self-inductances L and self-capacitances C as shown in Fig. 3. Between the resonators, there is either a mutual inductance L_m or a coupling capacitance C_m or both. Based on this circuit model, the coupling coefficient between the two resonators (or two degenerate modes in dual-mode filters) is usually given as [4, 31]:

$$k = \frac{\left(f_2^2 - f_1^2\right)}{\left(f_2^2 + f_1^2\right)} \tag{6}$$

or simply as [6] $\Delta f/f_o$ where f_1 and f_2 are the two splitting resonant frequencies, Δf is the difference between them and f_o is the center frequency. When the coupling between two resonators or two modes is stronger (over-coupled), it can be seen that Equation (6) is useful. However, when the coupling is close to critical, its error becomes larger. At critical coupling, i.e., when $f_1 = f_2$, the value of the coupling $k = 0$ can not be valid. In realizing NB microwave filters with a fractional bandwidth of less than 1%, a very weak coupling between two resonators (or modes) is required. If the quality factor Q of planar resonators is not relatively too high, the coupling coefficient extracted by Equation (6) would lead to a larger error in filter design. Therefore, the rigorous calculation of the coupling coefficient between two resonator modes must take the circuit loss into account as shown in the equivalent lumped-element circuit (see Fig. 3) where the self-circuit resistance R_o and the external loaded resistance R_e are included.

To simplify the analysis, only one type of coupling is considered, say the mutual coupling inductance L_m. However, it should be noted that the final expression derived for calculating the coupling coefficient, based on this assumption is also valid for the capacitance coupling or the mixed coupling structures shown in Figs. 4(a), (b), respectively. Note that Fig. 3 is just for a dual-mode filter (with a single resonator) cited to introduce the coupling types used in model, while the standard equivalent circuits of Fig. 2 and Fig. 4, used throughout the article are for standard 2-pole filters (with 2 resonators not a dual-mode single resonator filter).

At resonance, the imaginary part of the equivalent impedance Z_t between $TT^{'}$ points should be zero, so the following equation can be obtained [32]:

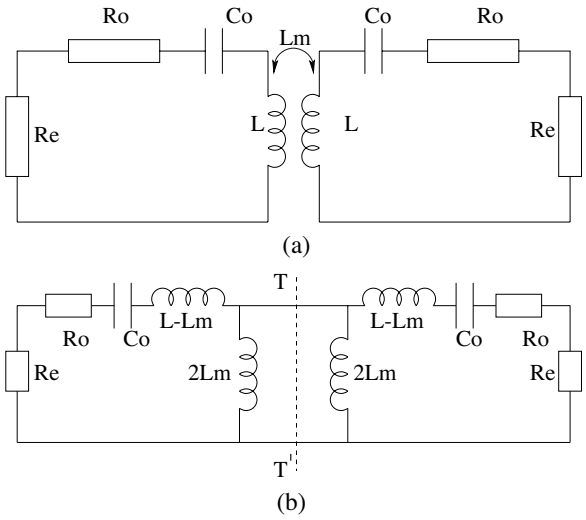

Figure 3. Equivalent lumped-element circuit of a dual-mode 2-pole bandpass filter with magnetic coupling only, used for the analysis.

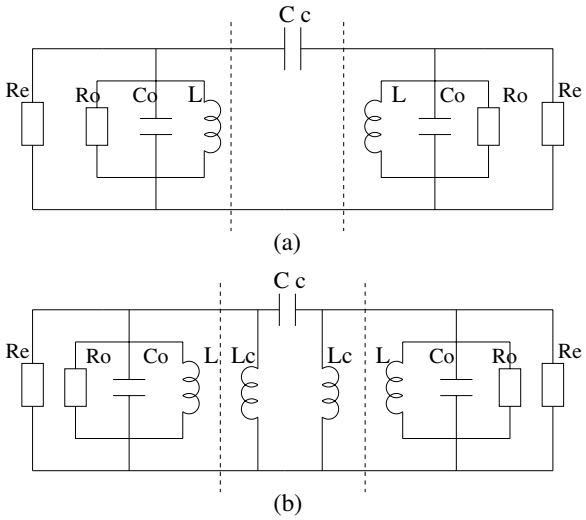

Figure 4. Equivalent lumped-element circuit of a standard 2-pole bandpass filter. (a) With capacitive coupling. (b) With mixed coupling.

$$\left(\frac{1}{Q}\right)^2 + 1 - k^2 + \left(\frac{f_o}{f}\right)^4 - 2\left(\frac{f_o}{f}\right)^2 = 0 \tag{7}$$

where:

$$k = \frac{L_m}{L}$$
$$f_o = \frac{1}{2\pi\sqrt{LC}}$$
$$\frac{1}{Q} = \frac{1}{Q_o} + \frac{1}{Q_e} \approx \frac{R_o}{\omega_o L} + \frac{R_e}{\omega_o L}$$

Q_o is the unloaded quality factor and Q_e is the external quality factor of the resonator. The solution of Equation (7) is:

$$\left(\frac{f_o}{f_{1,2}}\right)^2 = 1 \pm \sqrt{k^2 - \frac{1}{Q^2}} \tag{8}$$

When $k > \frac{1}{Q}$, the coupling coefficient obtained from the above formula (lets depict it as k_1) is:

$$k_1 = \sqrt{\left[\frac{\left(f_1^2 - f_2^2\right)}{\left(f_1^2 + f_2^2\right)}\right]^2 + \frac{1}{Q^2}} \tag{9}$$

Equation (9) shows that when $f_1 = f_2$, $k_1 = \frac{1}{Q}$, i.e., the critical coupling case where the split frequencies overlap.

3.1. Validation of the Model

The relative error calculated from (6) and (9), respectively is shown in Fig. 5. It can be observed that the relative errors are 35%, 100% and ∞, when $k_1 = \frac{1.5}{Q}$, $\frac{1.2}{Q}$ and $\frac{1}{Q}$, respectively. Only when $k_1 > \frac{3.4}{Q}$, it becomes less than 5%. If the two split frequencies (f_1 and f_2) and the Q-factor are found from a filter response either by measurement or EM simulation tool, the accurate coupling coefficient can easily be extracted using Equation (9). A dual-mode filter similar to a tested and reported one in a previous work [7] but with one zigzag step only and a suspended stripline configuration (dielectric substrate thickness $h = 1\,\text{mm}$, $\varepsilon_r = 2.8$ and operating frequency $f_o = 1.19\,\text{GHz}$ is designed and tested with conventional conductors for this purpose.

The coupling coefficients, extracted from Equations (6) and (9) are plotted versus d/w in Fig. 6, where d is the mode-modifying patch size normalized to the conductor width w. The two coefficients converge as the patch size (controlling the coupling) increases and diverge when it decreases. Another verification for the model is made using a

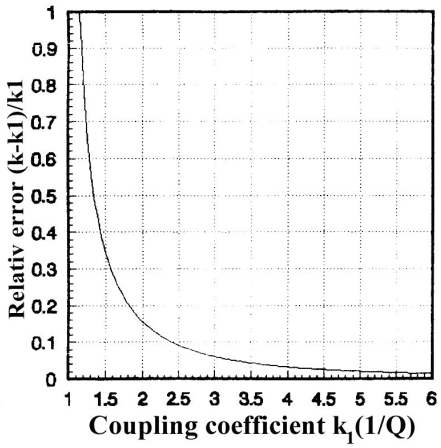

Figure 5. Relative error of the coupling coefficient computed from (6) and (9).

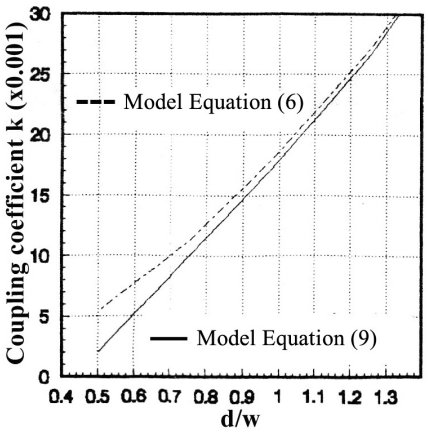

Figure 6. Coupling coefficients of a dual-mode experimental suspended microstrip filter extracted by (6) and (9) versus the mode-modifying patch size normalized to conductor width.

standard 2-pole filter where the separation between the resonators is believed to be dominant for controlling the coupling coefficients. The separation in the example filter reported in [28], is varied and the split frequencies can be seen in the computed transmission frequency responses illustrated in Fig. 7. The extracted coupling coefficients (using (6) and (9)) versus (S/w) are also presented in Fig. 8, where

the coupling coefficients of the two models become almost identical at higher values as the separation between the two resonators becomes very tight. However, they diverge exponentially as they become very weak. It can be seen that when the two split frequencies overlap at $S/w = 4.5$, the coupling coefficient from the standard model (6) approaches zero as mentioned above. However, the discrepancy of the two coupling values in this example, is much smaller than the previous one because of the much higher quality factor for such a fictitious HTS filter. Also, it can be observed from Fig. 6 and Fig. 8 that the decay of the coupling in the dual-mode filter is almost linear, while in the standard filter is exponential. This may be due to the different configurations and coupling structures of the two filters.

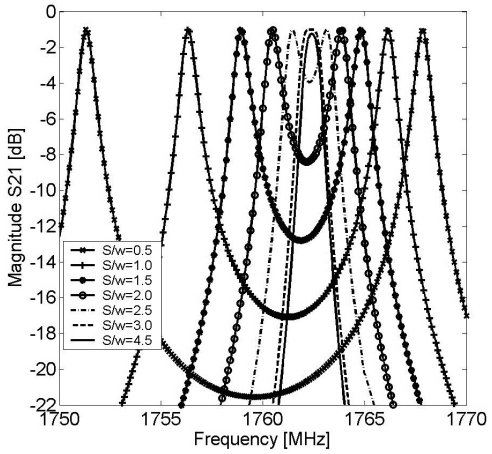

Figure 7. The split frequencies of the example filter [28] versus the ratio of separation S to conductor width w. The solid line is when the frequencies overlap.

4. MICROSTRIP DESIGN AND OPTIMIZATION OF THE FILTERS

4.1. Geometry for Minimizing the Coupling Coefficient

It is known [33] that arbitrary bends shown in Fig. 9 can be presented in a general equivalent circuit shown in Fig. 10(a). The mutual interaction between the two segments is expressed by M_{12} and M_{21}, as shown in Fig. 10(b). The total inductance general formula for a return circuit bend such as that shown in Fig. 9(a) with acute angle ψ is:

$$L_t = L_1 + L_2 - 2M_{12} \tag{10}$$

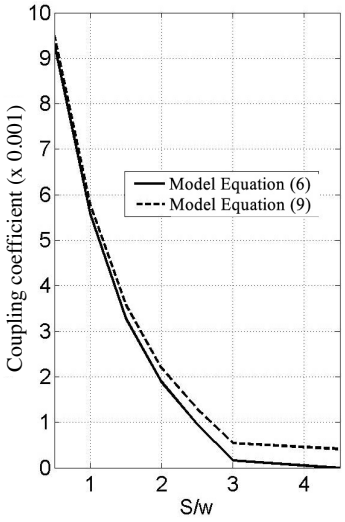

Figure 8. The extracted coupling coefficients (using (6) and (9)) of the example filter [28] versus the separation normalized to conductor width.

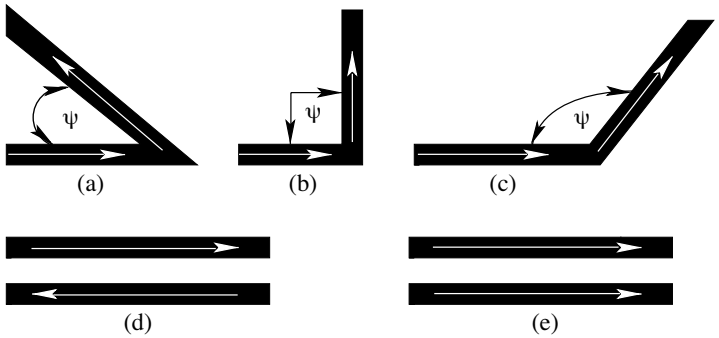

Figure 9. Arbitrary bent composed of two segments with different angles and current directions. The arrows in (a), (b), (c), (d) and (e) show the current directions in the segments.

where $M_{12} = M_{21}$ when the current in both segments has the same frequency. L_1 and L_2 are their self-inductances, respectively. The total inductance is less than the sum of their self-inductances. As ψ increases to 90°, M_{12} decreases to zero, i.e., the mutually induced electromagnetic fields (EMFs) vanish. In passing from an acute angle to an obtuse angle M_{12} changes sign and becomes a negative quantity so as to give greater total inductance than the sum of the self-

inductances and hence:

$$L_t = L_1 + L_2 - (-2M_{12}) = L_1 + L_2 + 2M_{12} \tag{11}$$

In the series combinations, Figs. 9(a), (b), (c), the effect of the angle ψ is dominant. In the parallel segments (see Figs. 9(d), (e), the effect of the current direction is dominant. When the current direction in both segments is identical, their mutual inductance $2M_{12}$ is to be added but when the current flows in opposite directions, $2M_{12}$ is to be subtracted. In light of these considerations, a new class of resonator structure can be designed with minimum parasitic mutual field interactions between its internal segments. Such a resonator should be composed of right-angle bends and parallel segments with opposite current directions where possible. If the inter-resonator coupling of a filter is forced to occur in regions with minimum current strength, it can be expected to have a filter with extremely small overall coupling coefficient, hence an ultra NB performance.

In microstrip configuration, the geometry and current directions of such a structure is shown in Fig. 11(a). Lets call it folded spiral in contrast to the conventional spiral geometry shown in Fig. 11(b), where all adjacent parallel lines have identical current directions (see the arrows). The circled locations highlight the would be current peak regions in each resonator.

Another structures are proposed, where the current flows in opposite directions in all of the adjacent parallel and horizontal segments. Such structures would make a significant difference from the conventional [12] doubly-meandered resonator structure, if (in addition to opposite current directions) the current peaks in adjacent resonators are located as far away as possible from each other. The proposed filter structures in Figs. 12(a), (b), (c) have regions of current peaks at various distances from each other, but all adjacent parallel and horizontal internal segments have opposite current directions.

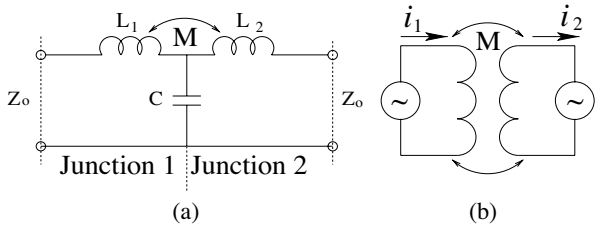

Figure 10. (a) Equivalent circuit of two segments. (b) Mutual inductance between two segments with equal current source and frequency.

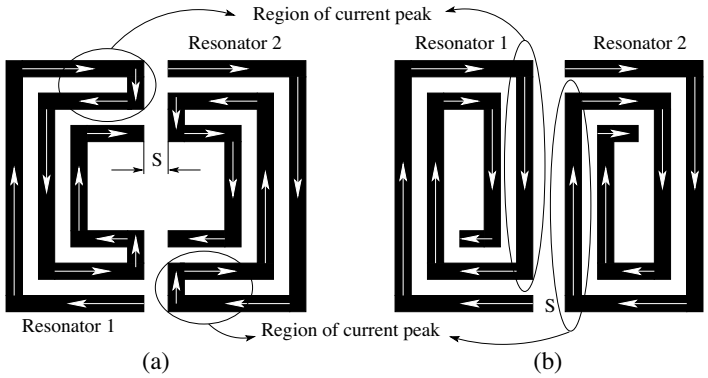

Figure 11. Comparison of current peak regions and directions between the proposed folded-spiral structure and the conventional spiral. (a) The proposed folded-spiral filter structure. (b) The conventional spiral filter structure.

In higher order than 2-pole filters, it is relatively easy to implement and control negative cross-couplings between non-adjacent resonators to realize a quasi-elliptic response, unlike a 2-pole filter except in the case of a 2-pole dual-mode filter [7]. Therefore, an optimization process is developed and simplified to only one parameter for the EM simulation tool to achieve a quasi-elliptic response in a faster and efficient way. This single parameter is the separation between resonators S.

The design procedure can be summarized in two steps: Firstly, the desired conductor width w and a first-cut ($\lambda/2$ resonator) physical length l_s of a straight microstrip line satisfying the specified center frequency (chosen to be $f_o = 1764\,\text{MHz}$) are calculated using standard formulas or AppCAD software [34] for the applied substrate parameters. These are chosen to be $LaAlO_3$ with $\varepsilon_r = 24$, $\tan\delta = 5 \times 10^{-5}$ and a thickness of $h = 0.5\,\text{mm}$. In the present case a $50\,\Omega$ uniform line width of $w = 0.180\,\text{mm}$ is used.

Secondly, the resonator line is shaped to the desired geometry until the calculated length is satisfied. Each resonator should be accommodated in an area of half a square, so that if the separation between them is reduced to zero, they form an exact square. However, due to the multiple bends and proximity effect of the various sections in these structures, the actual resonator length is somewhat different from the straight resonator length. Thus, it may be adjusted to resonate at the specified f_o by few iterations of pre-analyze with the EM tool. Once the center frequency of the filter is achieved, the only parameter to be

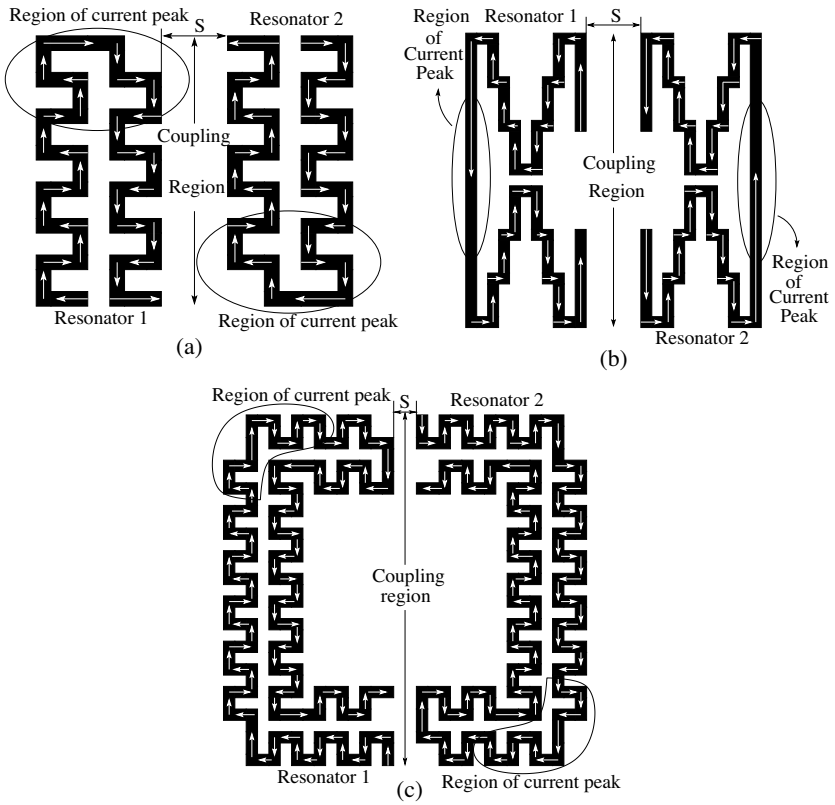

Figure 12. Proposed filter structures with regions of current peaks at various distances and opposite current directions in all adjacent parallel and horizontal segments. (a) Doubly-meandered line filter. (b) Step-wise meandered line filter. (c) Meandered folded-spiral filter.

optimized is the separation S, where the bandwidth and transmission zeros are controlled until a flat acceptable (to the specified ripple) passband is satisfied, regardless of the resulted optimum separation.

4.2. Optimization of the New Filters

One may select one or multiple parameters to optimize a structure. For each selected parameter, minimum and maximum bounds must be specified. The analysis limits the parameters to values within these bounds. The number of iterations must be also specified (as a maximum measure of control over the process). For each iteration, EM selects a value for each of the parameters included in the optimization,

then analyzes the circuit at each frequency specified in the objectives. Depending on the complexity of the circuit, the number of analysis frequencies and parameter combinations, an optimization may take a significant amount of processing time. Thus, minimizing the parameter combinations is crucial to minimize the processing time. An optimization can stop after fewer iterations (using a conjugate gradient method) if the optimization goal is achieved or no improvement in the error is found [30]. In this work, the optimization process is reduced to only one parameter, the separation S.

A nominal value of the optimization parameter may be chosen to be at least one conductor width. A maximum range of 10 widths may be sufficient. An anchored parameter allows to fix one end of a parameter then vary its length extending from that fixed point (anchor). In our case, one of the two resonators can be highlighted as a dependent parameter, i.e., to move with the corresponding box wall when extending the separation parameter.

Each design has a different location of the current peaks from the coupling region. In all the designs, the goal is to achieve the best possible passband shape in each filter structure to compare their bandwidths and the resulted optimum separation. The aim of this comparison is to explore the effects of current peak separation from each other and away from the coupling region on the bandwidth. All the new designs (except the conventional spiral which is for comparison only) have minimum internal parasitic couplings in regard of their internal opposite current directions.

The final layouts of the optimized filters with their input/output ports and shield walls are shown in Figs. 13(a), (b), (c), (d), (e) where Figs. 13(a), (b), (c), (d) show the meandered folded-spiral filter, the folded-spiral filter, the doubly-meandered line filter and the step-wise meandered line filter, respectively. Fig. 13(e) shows a conventional spiral filter for comparison. The resonator separations S of the filters are optimized for the best possible flatness of the passband, i.e., for a specified goal of 0.1 dB ripple. The box heights of all the filters are set to be identical $H = 3\,\text{mm}$.

5. MODELING AND SIMULATION RESULTS

Network (circuit model) and full-wave EM sonnet simulators are used in the analysis. The network and full-wave insertion IL responses of the modeled Chebychev and all the investigated quasi-elliptic 2-pole microstrip filter layouts (see Figs. 13(a), (b), (c), (d), (e)) are compared in Fig. 14 where the sharp differences in the out-of-band rejection and locations of transmission zeros of the various designs can be observed.

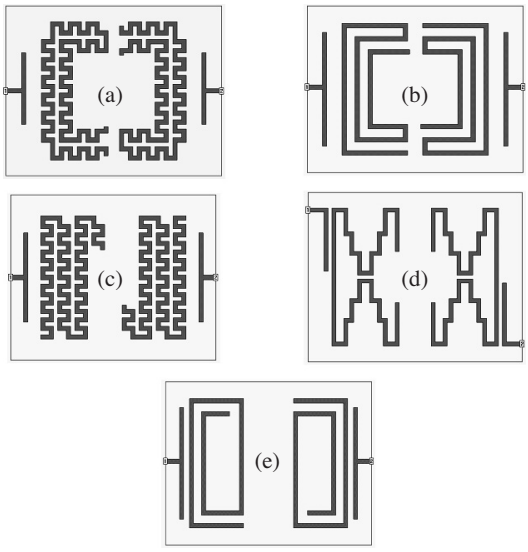

Figure 13. Final layouts of the new filters. (a) The meandered folded-spiral filter. (b) The folded-spiral filter. (c) The doubly-meandered line filter. (d) The step-wise meandered line filter. (e) A conventional spiral filter for comparison.

Close inspection of the IL and RL responses in the passband region of the filters can be clearly seen in Figs. 15(a), (b). Key parameter values of the microstrip filters, hardly observed on the response plots, are summarized in Table 1. These are the values of FBW, IL, RL and the coupling factors (the standard k and the modeled k_1. The ratio of the optimized separation normalized to conductor width is depicted in the table as S/w. From the responses of all the filters and Table 1, it can be observed that extremely narrowbands of 0.05% and 0.02% are achieved by the filter layouts a and b, respectively. Such FBWs may have not been reported previously for similar microstrip filter configurations.

In comparison with a computed filter such as the one shown in Fig. 1(g), an improvement of 73 and 29 times is achieved with filter a and b, respectively. In comparison with the best reported NB filters, the improvement may be estimated from 20 to 10 times respectively. However, it should be noted that the narrower the FBW, the larger the IL and the worse the RL. On the other hand, the narrower the FBW, the smaller the separation between resonators, i.e., better compactness. Thus, the disadvantages can be justified if the prime requirements of some critical applications are ultra NB response, sharp selectivity and

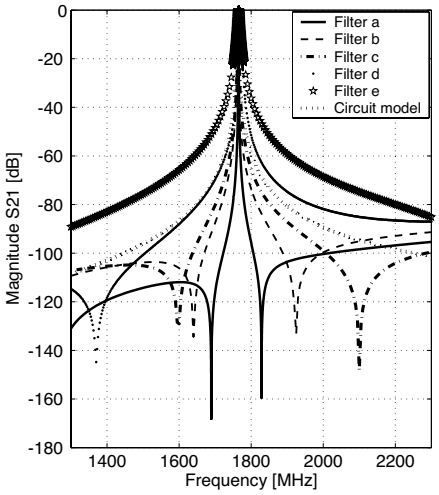

Figure 14. A wide-band IL responses of all the microstrip filters and the circuit model.

highly compact size as the case in wireless communications industry.

To gain a better feeling of the magnetic field strength distributed along the various parts of the half-wave resonators and hence their effect on the parasitic internal couplings and inter-resonator couplings, the current distributions on all the optimized microstrip filters are computed at the midband frequency and presented in Figs. 16(a), (b), (c), (d), (e).

Table 1. Extracted parameter results of all the microstrip filters shown in Figs. 13(a), (b), (c), (d), (e).

Layouts	$FBW\%$ 3 dB	$IL\,(f_o)$ (dB)	$RL\,(f_o)$ (dB)	$k\times$ 10^{-3}	$k_1\times$ 10^{-3}	S/w
Filter a	0.02	3.4	8.0	0.14	0.20	2.43
Filter b	0.05	1.0	17.5	0.22	0.45	3.40
Filter c	0.088	0.68	27.48	0.28	0.68	4.11
Filter d	0.14	0.43	36.4	1.35	2.00	8.0
Filter e	0.50	0.11	19.23	1.53	2.26	12.16

Inspecting the location of the current peaks on each filter and Table 1 having in mind the current directions within the filters (see

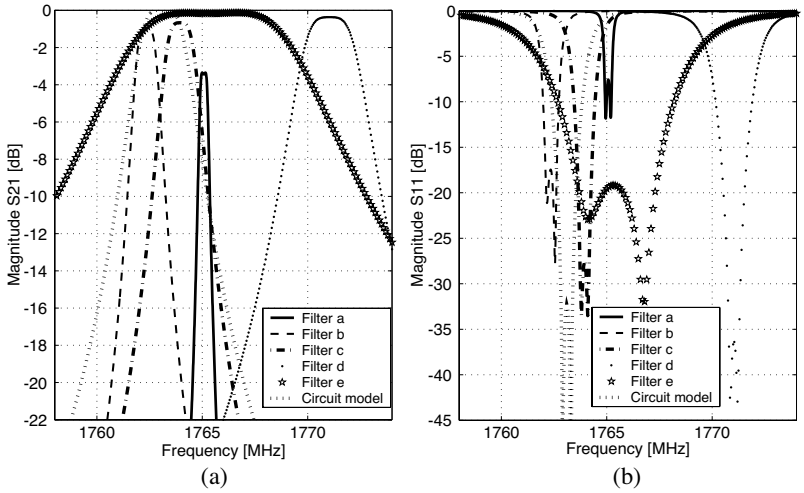

Figure 15. (a) A limited-band IL and (b) RL responses of all the filters plotted in Fig. 14 for close observation of their passband regions.

Figs. 11 and 12), it can be understood why filter e has the largest FBW and largest coupling value, although it has the largest separation S. This also explains why filter a has the narrowest FBW and smallest coupling value, while it has the smallest S. As can be seen from filter e, the sections with current maxima on each resonator are closest to each other (face-to-face), while the sections with current maxima on filter a are farthest from each other diagonally (top-left and bottom-right regions). This principle applies for the other three filters b, c and d.

6. EXPERIMENTAL AND DISCUSSION

From previous experience [7] and a plenty of published full-wave simulation and experimental data [13–16, 25] using the same materials and EM software, it can be noted that the modeling and simulation results are expected to agree well with tests but with a relative deterioration into the IL, RL, and the FBW. This shall presumably due to extraneous factors that could not be accounted for in the simulations such as fabrication tolerance, coaxial to microstrip transition matching, cooling medium, contraction of circuits at low temperature, material quality and contact interfaces (e.g., metal/HTS). In critical applications, however, additional tuning circuitry may be needed, though the complexity and size of the devices would be affected.

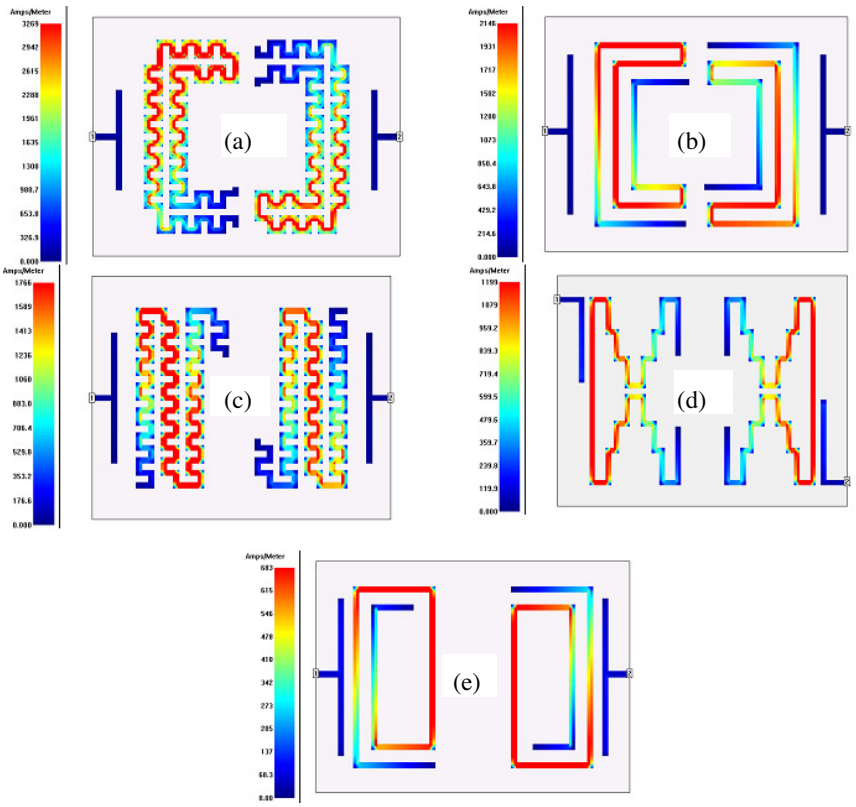

Figure 16. Current distribution on all of the microstrip filters computed at the midband frequency.

6.1. Fabrication and Measurements of Two Sample HTS Filters

Two sample Microstrip filters were fabricated on $LaAlO_3$ substrate with HTS YBCO film. The substrate and YBCO film are 508 µm (20 mil) and 0.6 µm (6000Å) thick, respectively. The HTS has a $T_C = 90.8$ K and a $\Delta T_C = 0.34$ K. The filters were fabricated using conventional integrated circuit processing techniques in the Microfabrication Facility at the NASA Glenn Research Center's Communication Technology Division. The filters were then characterized using a cryo station and HP 8510 VNA. A photograph of the fabricated HTS thin film sample filters e and b are show in Figs. 17(a), (b). A test fixture was developed to secure and enclose the microstrip filters during the measurements. The test fixture and a filter

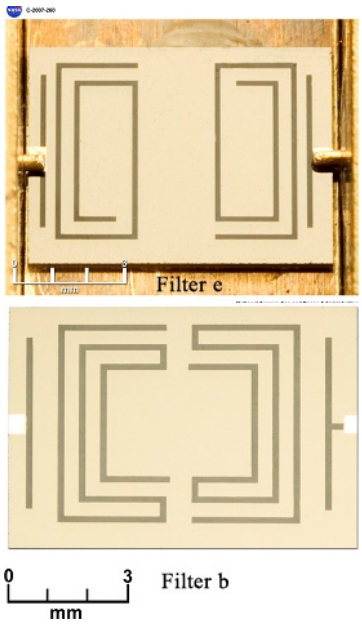

Figure 17. A photograph of the fabricated HTS thin film filter samples e and b.

sample embedded in it, are shown in Figs. 18(a), (b). The test fixture was milled from brass. SMA connectors were inserted through the sides of the fixture to allow the center conductor pin to make a contact with the microstrip feed line as shown in the figure. A short-open-load-thru (SOLT) calibration was performed to the system before measurements. This method of characterization, however, does not account for possible mismatch losses occurring at the interface transition: SMA center conductor-to-microstrip feedline. A more accurate approach would be to use on-wafer calibration standards and ground-signal ground-probes. However, this type of system (may be more convenient for open coplanar waveguide structures) was not available for the present microstrip filters. Therefore, just only two samples are tested to avoid wasting HTS materials with the same fault but to gain a sense of a real filter performance if the fault is removed.

The Measured and simulated transmission responses of filter e are plotted at wider and smaller frequency ranges in Figs. 19(a), (b). A good agreement between the responses is observed with center frequency, bandwidth and shape. However, the insertion loss of the tested filter is deteriorated with nearly 2 dB presumably due to the

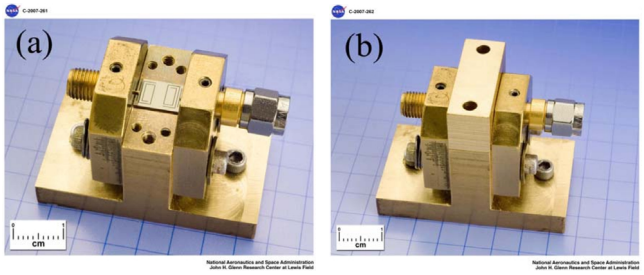

Figure 18. A photograph of the developed test fixture and a fabricated filter sample embedded in it. (a) Open fixture to view the SMA-feedline interface. (b) Closed fixture prior testing to minimize radiation losses.

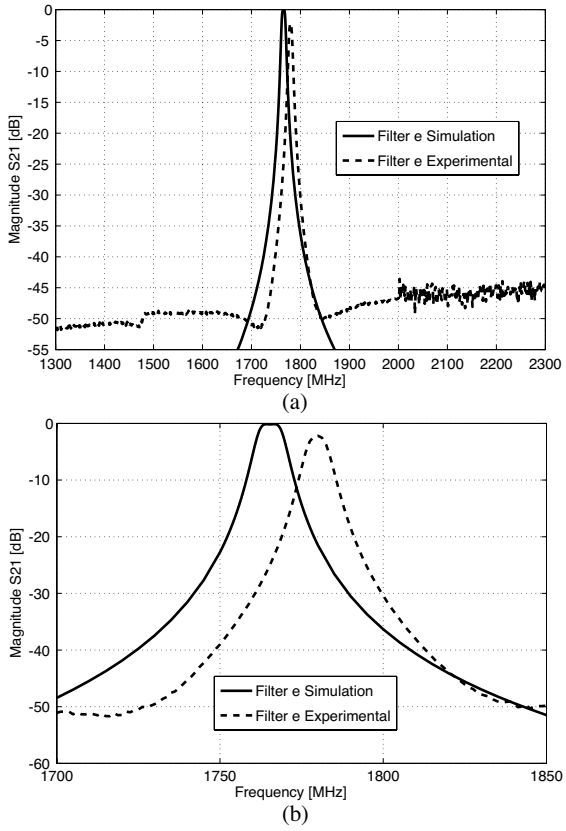

Figure 19. Measured and simulated transmission responses of filter e. (a) At wider frequency range. (b) At smaller range.

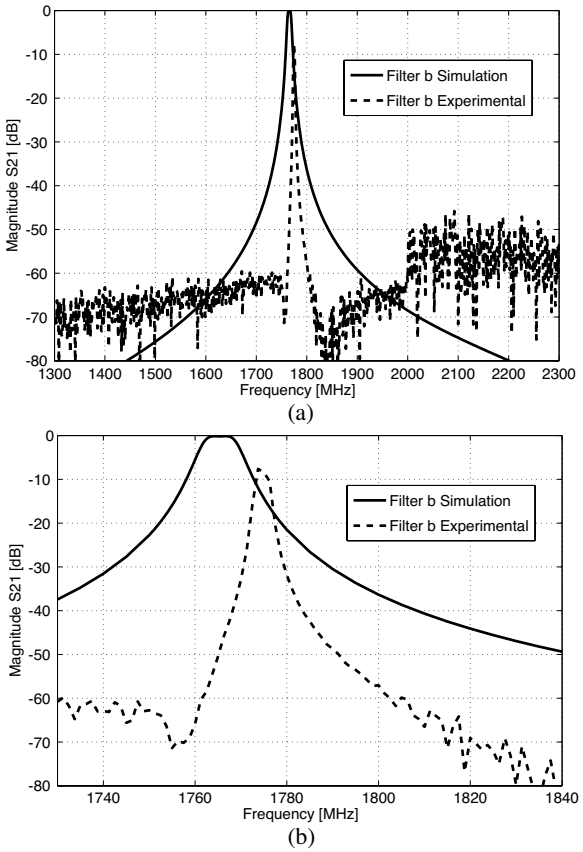

Figure 20. Measured and simulated transmission responses of filter b. (a) At wider frequency range. (b) At smaller range.

mismatch losses at the interface with the external circuitry. It may also be due to the different dimensions of the test fixture from the originally optimized box shield. The same effect on the insertion loss is also displayed with the test filter b, although it shows a much better selectivity with sharper response skirts than the simulated as can be seen in Figs. 20(a), (b). Both filters demonstrated transmission zeros near the passband. Note that the EM simulations for HTS models don't take the circuit losses into account but the dielectric substrate los tangent only assuming lossless conductors. Furthermore, the models don't take into account the low temperature test environment which usually causes contraction to the original circuits and hence a slight shift in center frequencies toward the higher side.

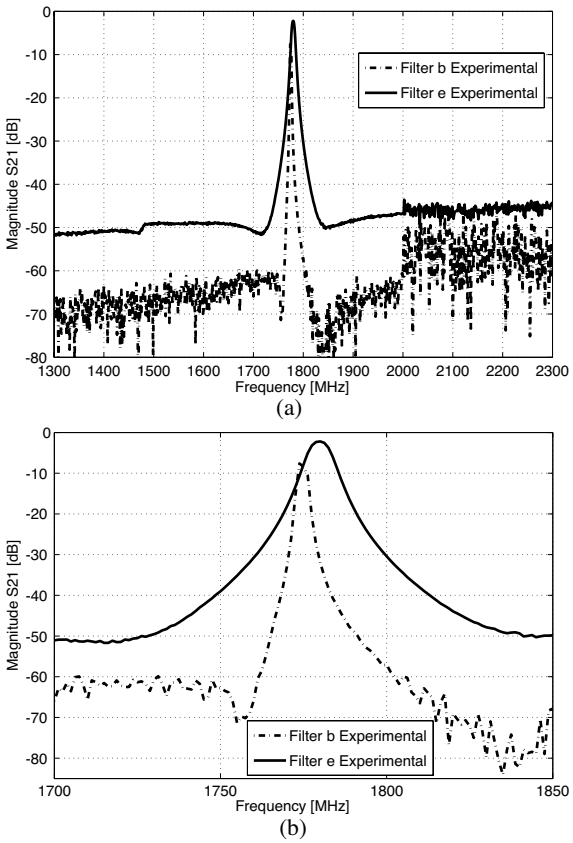

Figure 21. Response of the two measured filters e & b. (a) At wide frequency range. (b) At small frequency range. The sharper skirts and steeper transmission zeros of filter b is clearly observed, though the higher insertion loss, may due to the coax-feed line mismatch and a certain fabrication tolerance, is more obvious in (b).

To have a better sense of the improvement achieved in the new filter design b over the conventional design (filter e), a comparison plot of only the measured results of both filters e and b is shown in Figs. 21(a), (b). The sharper skirts and steeper transmission zeros of filter b is clearly observed, though the deteriorated insertion loss, is possibly due to the coax-feed line mismatch and poor shielding of test platform. These two measured filters and the simulated others, show that the concept of achieving ultra NB performance with still ultra compact size is valid. Refining fabrication of miniature shield box and using better on-wafer matching standards and/or tuning device,

may result in excellent practical filters with more than tens of times improvement in NB performance compared with similar configuration filters and materials.

7. CONCLUSION

A new class of microstrip filters were designed, optimized, measured and compared for ultra NB performance, essential to the wireless industry applications. The new designs demonstrated minimum parasitic couplings within the resonators and a minimum inter-resonator coupling despite a tighter separation between them. The new geometrical approach showed a crucial effect on the bandwidth performance and compactness. A good agreement between the simulated and measured responses was observed with center frequency, sharp selectivity, quasi-elliptic response, bandwidth and shape. However the insertion loss of the tested filter was deteriorated with nearly 2 dBs presumably due to the mismatch losses at the contact pads interface with the external circuitry and the poor shielding effect of the test platform. The best new designs showed a fractional bandwidth with tens of times of order narrower than previously reported similar passive configuration filters and materials. However, the study and measurements showed that the narrower the FBW, the larger the cost in IL and RL. Refining fabrication of miniature shield box (instead of test fixture) and using better on-wafer matching standards, and tighter contact pads, may improve the measurements. Such filters with extremely narrowband performance are useful for critical applications. A coupling coefficient model, with the losses taken into account, was also discussed. This model would be useful in NB filter design where a very weak coupling is needed when the Q is relatively low.

REFERENCES

1. Mtthaei, G. L., N. O. Fenzi, R. J. Forse, and S. M. Rohlfing, "Hairpin-comp filter for HTS and other narrow-band applications," *IEEE Transactions on Microwave Theory and Techniques*, Vol. 45, No. 8, 1226–1231, 1997.
2. Hong, J.-S. and M. J. Lancaster, "Cross-coupled microstrip hairpin-resonator filters," *IEEE Transactions on Microwave Theory and Techniques*, Vol. 46, No. 1, 118–122, 1998.
3. Yu, C.-C. and Y. K. Chang, "Novel compact elliptic-function narrow-band bandpass filters using microstrip open-loop resonators with coupled and crossing lines," *IEEE Transactions on Microwave Theory and Techniques*, Vol. 46, No. 7, 952–958, 1998.

4. Hong, J.-S. and M. J. Lancaster, "Aperture-coupled microstrip open-loop resonators and their applications to the design of novel microstrip bandpass filters," *IEEE Transactions on Microwave Theory and Techniques*, Vol. 47, No. 9, 1848–1855, 1999.
5. Hong, J.-S., M. J. Lancaster, D. Jedamzik, and R. B. Greed, "On the development of superconducting microstrip filters for mobile communications applications," *IEEE Transactions on Microwave Theory and Techniques*, Vol. 47, No. 9, 1656–1663, 1999.
6. Kim, H. T., B.-C. Min, Y.-H. Choi, S.-H. Moon, S.-M. Lee, B. Oh, J.-T. Lee, I. Park, and C.-C. Shin, "A compact narrowband HTS microstrip filter for PCS applications," *IEEE Transactions on Applied Superconductivity*, Vol. 9, No. 2, 3909–3912, 1999.
7. Hejazi, Z. M., P. S. Excell, and Z. Jiang, "Compact dual-mode filters for HTS satellite communication systems," *IEEE Microwave and Guided Wave Letters*, Vol. 8, No. 8, 275–277, 1998.
8. Hejazi, Z. M., Z. Jiang, and P. S. Excell, "Lumped-element microstrip narrow bandpass tunable filter using varactor-loaded inductors," *International Journal of Electronics*, Vol. 90, No. 1, 57–63, 2003.
9. Jeon, B. K., J. H. Kim, C. J. Lee, B. C. Min, Y. H. Choi, S. K. Kim, and B. Oh, "A novel HTS microstrip quasi-elliptic function bandpass filter using pseudo-lumped element resonator," *IEEE MTT-S International Microwave Symposium Digest*, Vol. 2, 1197–1200, 2000.
10. Reppel, M., "Novel HTS microstrip resonator configurations for microwave bandpass filters," Doctoral dissertation, Bergish University, Wuppertal, Germany, 2000.
11. Vendik, I. B., A. N. Deleniv, V. O. Sherman, A. A. Svishchev, V. V. Kondratiev, D. V. Kholodniak, A. V. Lapshin, P. N. Yudin, B.-C. Min, Y. H. Choi, and B. Oh, "Narrowband Y-Ba-Cu-O filter with quasi-elliptic characteristic," *IEEE Transactions on Applied Superconductivity*, Vol. 11, No. 1, 477–480, 2001.
12. Matthaei, G. L., "Narrow-band, fixed-tuned, and tunable bandpass filters with zig-zag hairpin-comb resonators," *IEEE Transactions on Microwave Theory and Techniques*, Vol. 51, No. 4, 1214–1219, 2003.
13. Sheng, Y. and S. Carles, "New advances in HTS microstrip filter design," *IEEE MTT-S International Microwave Symposium Digest*, Vol. 3, 1885–1888, 2003.
14. Yi, H. R., S. K. Remillard, and A. Abdelmonem, "A superconducting thin film filter of very high wide-band rejection," *IEEE MTT-S International Microwave Symposium Digest*, Vol. 3,

1893–1896, 2003.

15. Dustakar, K. and S. Berkowitz, "An ultra-narrowband HTS bandpass filter," *IEEE MTT-S International Microwave Symposium Digest*, Vol. 3, 1881–1884, 2003.
16. Zhou, J., M. J. Lancaster, and F. Huang, "Superconducting microstrip filter using compact resonators with double-spiral inductors and interdigital capacitors," *IEEE MTT-S International Microwave Symposium Digest*, Vol. 3, 1889–1892, 2003.
17. Hasan, A. and A. E. Nadeem, "Novel microstrip hairpinline narrowband bandpass filter using via ground holes," *Progress In Electromagnetics Research*, PIER 78, 393–419, 2008.
18. Xiao, J.-K., S.-P. Li, and Y. Li, "Novel planar bandpass filters using single patch resonators with corner cuts," *Journal of Electromagnetic Waves and Applications*, Vol. 20, No. 11, 1481–1493, 2006.
19. Zhu, Y.-Z., Y.-J. Xie, and H. Feng, "Novel microstrip bandpass filters with transmission zeros," *Progress In Electromagnetics Research*, PIER 77, 29–41, 2007.
20. Xiao, J.-K. and Y. Li, "Novel microstrip square ring bandpass filters," *Journal of Electromagnetic Waves and Applications*, Vol. 20, No. 13, 1817–1826, 2006.
21. Zhao, L.-P., X.-W. Chen, and C.-H. Liang, "Novel design of dual-mode dual-band bandpass filter with triangular resonators," *Progress In Electromagnetics Research*, PIER 77, 417–424, 2007.
22. Xiao, J.-K., S.-W. Ma, S. Zhang, and Y. Li, "Novel compact split ring stepped impedance resonators (SIR) bandpass filters with transmission zeros," *Journal of Electromagnetic Waves and Applications*, Vol. 21, No. 3, 329–339, 2007.
23. Wang, Y. X., B-Z. Wang, and J. Wang, "A compact square loop dual-mode bandpass filter with wide stop-band," *Progress In Electromagnetics Research*, PIER 77, 67–73, 2007.
24. Xiao, J.-K., "Novel microstrip dual-mode bandpass filter using isosceles triangular patch resonator with fractal-shaped structure," *Journal of Electromagnetic Waves and Applications*, Vol. 21, No. 10, 1341–1351, 2007.
25. Moghadasi, S. M., A. R. Attari, and M. M. Mirsalehi, "Compact and wideband 1-D mushroom-like EBG filters," *Progress In Electromagnetics Research*, PIER 83, 323–333, 2008.
26. Wang, X.-H., B.-Z. Wang, and K. J. Chen, "Compact broadband dual-band bandpass filters using slotted ground structures," *Progress In Electromagnetics Research*, PIER 82, 151–166, 2008.

27. Naghshvarian-Jahromi, M. and M. Tayarani, "Miniature planar UWB bandpass filters with circular slots in ground," *Progress In Electromagnetics Research Letters*, Vol. 3, 87–93, 2008.
28. Hejazi, Z. M. and A. Omar, "Modeling and simulation of novel ultra-narrowband miniature microstrip filters for mobile and wireless critical applications," *Microwave & Optical Technology Letters*, Vol. 45, No. 1, 35–39, 2005.
29. Hejazi, Z. M. and Z. Jiang, "A new model to calculate the coupling coefficient for more accurate filter design and further development of narrowband-filter performance," *Microwave & Optical Technology Letters*, Vol. 47, No. 2, 180–185, 2005.
30. Sonnet User's manuals for em and related software, release 9. North Syracuse, NY, USA, Sonnet Software, Inc, 2003.
31. Grounds, P. W. and K. A. Zaki, "Analysis of the coupling between degenerate modes of enclosed rectangular microstrip patches," *Journal of Electromagnetic Waves and Applications*, Vol. 9, No. 11–12, 1503–1516, 1995.
32. Jiang, Z., Z. M. Hejazi, P. S. Excell, and W. Y. Xu, "A new HTS microwave filter using dual-mode multi-zigzag microstrip loop resonators," *IEEE Asia Pacific Microwave Conference*, Vol. 3, 813–816, Nov. 30–Dec. 3, 1999.
33. Hejazi, Z. M., "Superconducting planar resonators and filters," Doctoral dissertation, University of Bradford, Bradford, UK, 1998.
34. Agilant Rf and microwave appCAD software, www.hp.woodshot.com/appcad/appcad.htm, 2004.
35. Rautio, J. C. and V. Demir, "Microstrip conductor loss models for electromagnetic analysis," *IEEE Transactions on Microwave Theory and Techniques*, Vol. 51, No. 3, 915–921, 2003.
36. Matthaei, G. L., L. Young, and E. M. T. Jones, *Microwave Filters, Impedance Matching Networks, and Coupling Structures*, Norwood, Artech House, MA, 1980.